Spora: A Journal of Biomathematics

Volume 1 | Issue 1 Article 6

2015

Spontaneous Calcium Release in Cardiac Myocytes: Store Overload and Electrical Dynamics

Amanda M. Alexander
Western Washington University, alexana6@students.wwu.edu

Erin K. DeNardo
Washington University in St. Louis, denardoerink@wustl.edu

Eric Frazier III
La Salle University, fraziere3@student.lasalle.edu

Michael McCauley
University of Maryland, Baltimore County, mmich1@umbc.edu

Nicholas Rojina
University of North Carolina at Chapel Hill, norjina0@live.unc.edu

See next page for additional authors

Spontaneous Calcium Release in Cardiac Myocytes: Store Overload and Electrical Dynamics

Authors
Amanda M. Alexander, Erin K. DeNardo, Eric Frazier III, Michael McCauley, Nicholas Rojina, Zana Coulibaly, Bradford E. Peercy, and Leighton T. Izu

Intercollegiate Biomathematics Alliance

SPORA
A Journal of Biomathematics

Spontaneous Calcium Release in Cardiac Myocytes: Store Overload and Electrical Dynamics

Amanda M. Alexander[1], Erin K. DeNardo[2], Eric Frazier III[3], Michael McCauley[4], Nicholas Rojina[5], Zana Coulibaly[4], Bradford E. Peercy[4,*], Leighton T. Izu[6]

*Correspondence:
Prof. Bradford E. Peercy,
Dept. of Mathematics and Statistics,
University of Maryland,
Baltimore County,
1000 Hilltop Circle,
Baltimore, MD 21250, USA
bpeercy@umbc.edu

Abstract

Heart disease is the leading cause of mortality in the United States. One cause of heart arrhythmia is calcium (Ca^{2+}) mishandling in cardiac muscle cells. We adapt Izu's et al. mathematical reaction-diffusion model of calcium in cardiac muscle cells, or cardiomyocytes, [14], implemented by Gobbert [12], and analyzed in Coulibaly et al. [8] to include calcium being released from the sarcoplasmic reticulum (SR), the effects of buffers in the SR, particularly calsequestrin, and the effects of Ca^{2+} influx due to voltage across the cell membrane. Based on simulations of the model implemented in parallel using MPI, our findings aligned with known biological models and principles, giving us a thorough understanding of several factors that influence Ca^{2+} dynamics in cardiac myocytes. Specifically, dynamic calcium store will cap previous calcium blow-up seen in the model. Calcium channels located in spatial opposition of calcium release units produce more predictable intracellular calcium propagation. And we used multi-parametric calcium dynamics tables, which act as a multidimensional bifurcation diagram, to visualize parameter boundaries between different biophysical dynamics.

Keywords: differential equations, biology, mathematical models

1 Introduction

Every heartbeat requires the coordination of many subsystems in the heart cells including the electrical system, the Ca^{2+} control system, and the contractile system. This coordination is called excitation-contraction coupling [3]. The Ca^{2+} control system couples the electrical excitation and contraction of the myofibrils. Under normal conditions Ca^{2+} release into the cytosol is triggered by the action potential generated by the electrical system. However, a variety of conditions can result in Ca^{2+} being spontaneously (independent of the action potential) released. This spontaneous Ca^{2+} release can disrupt the electrical system and engender conditions that increase the propensity for cardiac arrhythmias [15], [4].

Arrhythmias remain a leading cause of morbidity and mortality in the United States [1]. Implantable electrical defibrillators have significantly reduced mortalities, but they do not prevent the onset of arrhythmias. Antiarrhythmic drug therapy has, except with a small handful of exceptions, been surprisingly ineffective [28], [22]. A better understanding of how Ca^{2+} handling goes awry is likely to provide new avenues for antiarrhythmic drug therapies. In this paper, we extend an earlier 3-dimensional stochastic model of Ca^{2+} handling [13], [14] to now include dependence of Ca^{2+} release on sarcoplasmic reticulum (SR) Ca^{2+} concentration and the electrical system. The main question is then can spontaneous calcium release arise and propagate when the Ca^{2+} level in the SR is dynamic as was shown in the static SR calcium case [8].

One aim in creating this model is to address the hypothesis that spontaneous Ca^{2+} release can feedback onto the electrical system via the sodium calcium exchanger to induce anomalous electrical activity such as delayed after depolarizations or early after depolarizations. Thus, adding in the sarcoplasmic reticulum component addresses having a dynamic driving force for calcium release events and including the electrical subsystem allows translation of the spontaneous calcium transients to changes in the transmembrane potential and potential arrhythmias.

[1]Department of Mathematics, Western Washington University, Bellingham, WA, [2]Department of Mathematics, Washington University, St. Louis, MO, [3]Department of Mathematics and Computer Science, La Salle University, Philadelphia, PA, [4]Department of Mathematics and Statistics, University of Maryland, Baltimore County, Baltimore, MD, [5]Department of Mathematics, University of North Carolina, Chapel Hill, NC, [6]Department of Pharmacology, University of California, Davis, Davis, CA

2 Background

The sarcoplasmic reticulum (SR) is the main Ca^{2+} storage organelle within cardiac myocytes. Local Ca^{2+} releases in cardiac myocytes are known as calcium sparks, and they are required for cardiac muscle contraction; these are elementary events that trigger global calcium release [7]. Ca^{2+} release units (CRUs) act as consortium of calcium-sensitive channels between the SR and the cytosol, and they are the pathway by which spark releases are made from the SR. The level of contractions of the heart are directly related to elevated Ca^{2+} levels, so a disruption in the diffusion of cytosolic calcium and its removal from the cell impairs the ability of cardiomyocytes to relax. The propagation of waves, exemplified in Figure 2.1, occurs due to the process of Ca^{2+}-induced-Ca^{2+}-release (CICR) [10] whereby the elevated level of Ca^{2+} from the extracellular space into the cytosol triggers CRUs to fire and release additional Ca^{2+} from the SR. The Ca^{2+} moving into the cytosolic space then acts as a messenger by increasing the concentration of cytosolic Ca^{2+} and therefore directly activating CICR and release of Ca^{2+} from the SR activating contraction [6] shown in Figure 2.2.

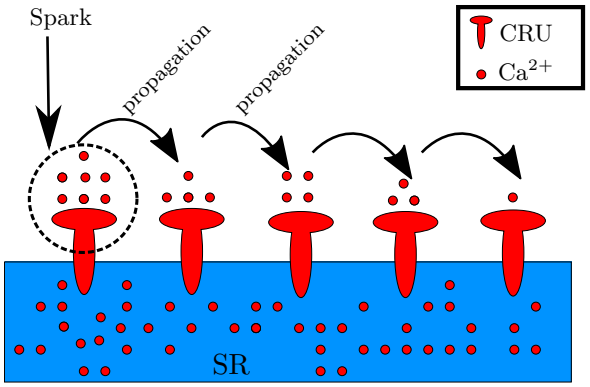

Figure 2.1: Triggering of Ca^{2+} waves. Calcium is spontaneously (or manually) elevated around a calcium release unit (CRU) as a calcium spark. Calcium diffuses to neighboring CRUs and, with sufficient concentration, opens them to release yet more calcium from the calcium stored in the sarcoplasmic reticulum (SR).

Spontaneous Ca^{2+} waves are typically observed during overload of Ca^{2+} concentration in the SR, causing depolarization of the cell membrane through the activation of sodium/calcium exchangers. Afterdepolarizations in membrane potential can occur when intracellular conditions depolarize the cell membrane to its threshold potential, inducing a spontaneous action potential [1] since Ca^{2+} channels activate on membrane depolarization responding to action potentials. These channels are responsible for converting the electrical signal provided by the action potential to the movement of Ca^{2+} into the cell.

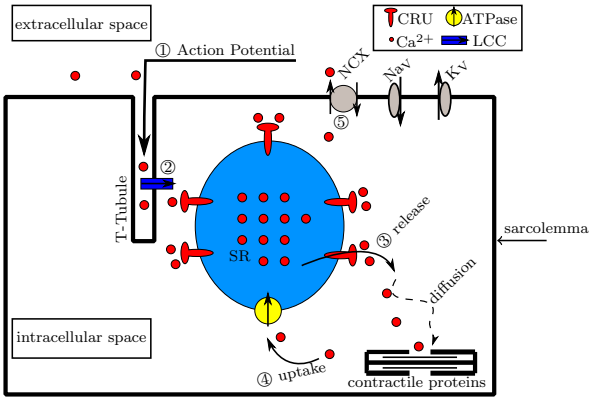

Figure 2.2: Diagram of cellular space. Invaginations of cell membrane in T-tubules allows close proximity of calcium channels (LCC) and calcium release units (CRUs) and efficient activation of CRUs by action potentials passed along with sodium (Na_v) and potassium (K_v) channels. Released calcium triggers muscle contraction and is taken back up into the SR via ATPases. Sodium calcium exchangers (NCX) remove calcium at the expense of bringing in sodium.

Extracellular calcium (Ca^{2+}) ions are necessary for contraction to occur in cardiac muscle cells [21]. Inward flow of a Ca^{2+} current is important in linking electrical and mechanical excitation in the cardiac muscle cells. The L-type calcium channel (LCC) in the plasma membrane, connecting the extracellular to the intracellular space, is responsible for the excitation-contraction coupling (ECC), the physiological process by which the electrical stimulus in the form of an action potential is converted to a mechanical response, the contraction of the heart [2].

SR Ca^{2+} release contributes the majority of Ca^{2+} for cytosolic contractile activation, and SR load critically regulates SR Ca^{2+} release during both ECC and spontaneous SR Ca^{2+} release. These conditions have the ability to cause delayed afterdepolarizations and arrhythmias [19]. Spontaneous Ca^{2+} waves are typically observed during overload of Ca^{2+} in the SR, causing depolarization of the cell membrane. Certain conditions allow the cell to reach the threshold for activation of spontaneous electrical activity. This occurs due to the induction of inward current by the Ca^{2+} waves produced.

Ca^{2+} buffering is a control system so as to slow down or regulate certain intracellular processes. It is the rapid binding of Ca^{2+} to other substances in a space in the cell. When the Ca^{2+} binds to buffers in order to form another compound, there is then a lower free Ca^{2+} concentration in the SR [11]. Calsequestrin is non-mobile and acts as

a major buffer in cardiac muscle cells by lowering the amount of unbound Ca^{2+} in the SR space [16].

In this paper, we present a mathematical model for studying certain conditions in cardiomyocytes in order to determine their role in resulting Ca^{2+} waves. Key elements to the model are the incorporation of the SR Ca^{2+} store and its Ca^{2+} flux through CRUs into the cell, buffer species in the SR, and a voltage model for current differences across the membrane so as to incorporate incoming Ca^{2+} from the extracellular space through LCCs.

3 Methodology

In this section we will write down the original model by Izu et al. [14] that has been created to study spontaneous calcium release in a 3-dimensional cardiac cell. Then we add in the dynamic SR. Finally, we tack on a voltage model by Morris-Lecar [18] as a simple way to relate transmembrane potential and calcium influx into the cell.

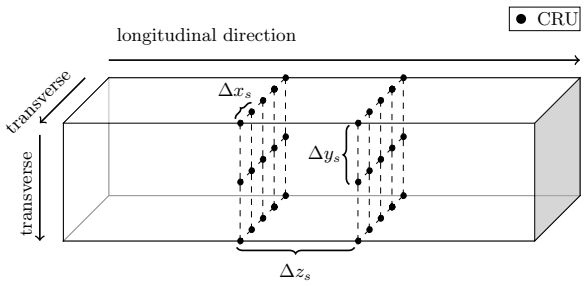

Figure 3.1: Our PDE domain. Each CRU is represented as a point source to emulate their role as point sources of Ca^{2+} with separation given by $(\Delta x_s, \Delta y_s, \Delta z_s)$.

In order to track the change in concentration of calcium and buffer species in the cytosol, we utilize the following system of partial differential equations [13, 14]:

$$\frac{\partial c}{\partial t} = \nabla \cdot (D_c \nabla c) + \sum_{i=1}^{nsc} R_i + J_{\text{CRU}} + J_{\text{leak}} - J_{\text{pump}}, \tag{3.1}$$

$$\frac{\partial b_i}{\partial t} = \nabla \cdot (D_{b_i} \nabla b_i) + R_i, \quad i \in \{1, \ldots, nsc\}, \tag{3.2}$$

$$R_i = -k_i^+ c b_i + k_i^-(b_{i_T} - b_i), i \in \{1, \ldots, nsc\}. \tag{3.3}$$

Equation (3.1) represents the change in calcium concentration, c, over time, equation (3.2) represents the change in each buffer species concentration, b_i, over time, and equation (3.3) represents the reaction of buffer species with calcium as it relates to both their concentrations. The first term in equation (3.1), $\nabla \cdot (D_c \nabla c)$, represents the diffusion of Ca^{2+} with diffusion coefficient matrix, D_c, which is slightly anisotropic due to the cellular structure. The second term, $\sum_{i=1}^{nsc} R_i$, is the sum of the reaction terms with forward and backward reaction rates k_i^+ and k_i^-, respectively, for each buffer species reacting with calcium, total buffer concentration, b_{i_T}, and buffer diffusion coefficient matrix, D_{b_i}. This term allows us to keep track of the calcium changes due to these reactions. We treat two cytosolic buffer species ($nsc = 2$) which can be roughly interpreted as a mobile fluourescent dye and immobile troponin molecules. The third term, J_{CRU}, represents the influx of calcium when the CRU opens and its opening probability is calcium dependent. The fourth term, J_{leak}, represents the leak of calcium from the SR into the cytosol that keeps the cell at equilibrium at basal level. The fifth term, J_{pump} represents the pumping of calcium into the SR. The mathematical equations representing these last three flux terms are below:

$$J_{pump} = V_{pump} \frac{c^{n_{pump}}}{K_{pump}^{n_{pump}} + c^{n_{pump}}}, \tag{3.4}$$

$$J_{leak} = V_{pump} \frac{c_0^{n_{pump}}}{K_{pump}^{n_{pump}} + c_0^{n_{pump}}}, \tag{3.5}$$

$$J_{CRU} = \sum_{i \in (x,y,z)} \hat{\sigma} \mathcal{O}(c) \delta(X - X_i), \tag{3.6}$$

$$\mathcal{O}(c) = \begin{cases} 1 & \text{if } \alpha \leq J_{prob}, \\ 0 & \text{if } \alpha > J_{prob}, \end{cases} \tag{3.7}$$

$$J_{prob} = P_{max} \frac{c^{n_{prob}}}{K_{prob_c}^{n_{prob}} + c^{n_{prob}}} \ . \tag{3.8}$$

Equations (3.4) and (3.5) are set up so that J_{pump} and J_{leak} balance each other when the calcium concentration is at basal level (i.e. no calcium from CRUs), but equation (3.4) can also balance out equation (3.6) when there is an increase in calcium due to CRUs opening. V_{pump} is the maximal pump rate and K_{pump} is the pump sensitivity. Equation (3.6) is comprised of three terms describing how much, when, and where calcium is released by the CRU. The first term represents how much calcium is released by the CRU, with $\hat{\sigma}$ being the constant maximum release rate of c into the cytosol. The second term is equation (3.7), the gating function, which is 0 if the CRU is closed and 1 if the CRU is open. To determine whether the CRU is open or closed, equation (3.8) calculates this probability based on calcium concentration and other constants determined from experimental data. This J_{prob} value is then compared to a random number α, uniformly distributed between 0 and 1, to determine if the CRU opens or stays closed. The third term $\delta(X - X_i)$ is used to model the CRU's as point sources of calcium in three dimensions, so that calcium is released at just X_i in our model.

3.1 SR Calcium

In the Izu model, implemented originally in [12] and further studied in [8], SR Ca^{2+} release depends only on the cytosolic Ca^{2+} concentration at the CRU but Ca^{2+} release also depends strongly on the SR Ca^{2+} concentration [23], [9]. To improve the current model we therefore included the dynamics for SR Ca^{2+} s and the SR Ca^{2+} buffers b_j and made the Ca^{2+} release depend on SR Ca^{2+}:

$$\frac{\partial s}{\partial t} = \nabla \cdot (D_s \nabla s) + \sum_{j=1}^{nss} R_j - \gamma(J_{CRU} + J_{leak} - J_{pump}), \tag{3.9}$$

$$\frac{\partial b_j}{\partial t} = \nabla \cdot (D_{b_j} \nabla b_j) + R_j. \tag{3.10}$$

The third set of terms (multiplied by γ) in equation (3.9) are identical to those in equation (3.1), but have opposite sign because Ca^{2+} is conserved between the SR and cytosolic compartments. Also note that γ represents the ratio of the volume of the cytosol to the volume of the SR to make the change in concentration of the SR account for its significantly smaller volume. For clarity, notice that the summing of reaction terms is changed to R_j to represent SR buffers, b_j. We will consider a single buffer specie calsequestrin ($nss = 1$). Now to actually have s influence CRU openings, we had to modify J_{CRU} and some of its terms as in the following:

$$J_{CRU} = \sum_{i \in ix,y,z} \left(\hat{\sigma} \frac{s - c}{s_0 - c_0} \right) \mathcal{O}(c, s) \delta(X - X_i), \tag{3.11}$$

$$J_{prob} = \frac{P_{max} \cdot c^{n_{prob}}}{K_{prob_c}^{n_{prob}} + c^{n_{prob}}} \cdot \frac{s^{n_{prob}}}{K_{prob_s}^{n_{prob}} + s^{n_{prob}}}. \tag{3.12}$$

Notice that in equation (3.11), there is change in the first term $\hat{\sigma}$ from being a constant maximum release rate to being affected by the concentrations of s and c with the fraction $(s-c)/(s_0-c_0)$ with $1/(s_0-c_0)$ to act as a scaling factor for comparison of $\hat{\sigma}$ with static SR simulations. The second term is equation (3.7), the gating function, which now has s as an input variable due to the extra term in equation (3.12). This extra term makes J_{prob} depend on SR calcium in such a way that when s is high the probability of the CRU opening is the same as it used to be but when s is low the probability of the CRU opening is much smaller.

3.2 Voltage Model

To be able to consider the impact of the electrical system, we introduced the Morris-Lecar voltage model, described below.

3.2.1 Morris-Lecar Model

We assume a simple conductance model for cardiomyocytes, using the model of a barnacle muscle fiber composed of voltage-dependent Ca^{2+} and K^+ channels. The introduction of current stimuli produce depolarizations

Parameters	Definition	Values/Units	Source
nsc	number of cytosol Ca^{2+} buffer species	2	[12]
b_{i_T}	total buffer concentration in cytosol	50,123 μM	[12]
D_c	cytosolic calcium diffusion coefficient matrix	diag(0.15,0.15,0.3)	[12]
D_{b_i}	cytosol buffer diffusion coefficient matrices (fluorescent, Troponin)	diag(0.01,0.01,0.02) μm^2/ms, diag(0.00,0.00,0.00) μm^2/ms	[5, 25]
k_i^+	forward reaction coefficients for buffer species	80e-3, 100e-3 $\mu M^{-1} ms^{-1}$	[12]
k_i^-	reverse reaction coefficients for buffer species	90e-3, 100e-3 ms^{-1}	[12]
V_{pump}	maximum pump rate	2-6 μM/ms	[8]
K_{pump}	pump sensitivity to Ca^{2+}	0.184 μM	[12]
n_{pump}	hill coefficient for pump function	4.0	[12]
n_{prob}	hill coefficient for probability function	1.6	[12]
c_0	initial cytosol calcium concentration	0.1 μM	[12]
X_i	three dimensional vector for CRU location	(X_x, X_y, X_z) μm	
$\hat{\sigma}$	maximum rate of release	100-200 $\mu M \mu m^3$/ms	[8]
P_{max}	maximum probability for release	0.3	[14]
K_{prob_c}	sensitivity of CRU to cytosol calcium	5-15 μM	[14]

Table 3.1: Parameter values for the original Izu model as implemented in [12] and [8].

across the cell membrane. Oscillations in voltage then begin to occur once the constant current stimulus reaches a certain threshold that is imposed by the model. Although external calcium concentration is particularly influential on the nature of the oscillatory behavior, oscillations only occur when both Ca^{2+} and K^+ currents are present and activated at the same time. Thus, the equation below for monitoring voltage has K^+ terms involved. In the same fashion as Morris and Lecar [18], we make use of the different relaxation times of the Ca^{2+} and K^+ conductances to study the oscillating state in some generality as shown below. We have also τ as a scaling factor for the Morris-Lecar model to adjust the action potential duration to extend the period of the model to more physiological periods of hundreds of milliseconds.

Equation (3.17), combined with the equations below, represents a nonlinear Hodgkin-Huxley-like equation, and explains the excitation of the cell by varying the transmembrane potential or voltage, V, in the cell along with auxiliary gating variables for calcium conductance, m, and potassium conductance, n, with assigned constants from experimental data. The auxiliary functions are

$$m_\infty(V) = \frac{1}{2}\left[1 + \tanh\left(\frac{V - V_1}{V_2}\right)\right], \tag{3.13}$$

$$n_\infty(V) = \frac{1}{2}\left[1 + \tanh\left(\frac{V - V_3}{V_4}\right)\right], \tag{3.14}$$

$$\lambda_n(V) = \overline{\lambda_n}\cosh\left(\frac{V - V_3}{2V_4}\right). \tag{3.15}$$

We study this reduced set of equations, in which the Ca^{2+} system is assumed to be so much faster than the K^+ system that calcium conductance is instantaneously in quasi steady state at all times so $m = m_\infty(V)$. [18]. The model for calcium then becomes

$$\frac{\partial c}{\partial t} = \nabla\cdot(D_c\nabla c) + \sum_{i=1}^{nsc} R_i + (J_{CRU} + J_{leak} - J_{pump}) + J_{LCC} + J_{mleak} - J_{mpump}. \tag{3.16}$$

The voltage and potassium gating variable equation are, respectively,

$$\frac{\partial V}{\partial t} = \tau\cdot\frac{1}{C}(I_{\text{app}} - g_L(V - V_L) - g_{Ca}m_\infty(V)(V - V_{Ca}) - g_K n(V - V_K)), \tag{3.17}$$

$$\frac{\partial n}{\partial t} = \tau\cdot\lambda_n(V)[n_\infty(V) - n]. \tag{3.18}$$

Now we see the effects of voltage on calcium dynamics through the J_{LCC} term and its related flux terms below, which are formulated to mirror the J_{pump} and J_{leak} terms from equations (3.4) and (3.5). Note that, due to a lack of evidence on the actual location of LCC channels, we have implemented two versions of our voltage model: one where Ca^{2+} flux from the LCC channels is only present across from the CRUs of the SR and one where Ca^{2+} flux from the LCC channels is present around the entire plasma membrane. In order to account for this difference, we multiply our J_{LCC} term by volume/(number of CRUs) $= (12.8\cdot 12.8\cdot 64)/6975 = 1.503$ when we assume LCC channels are around the entire plasma membrane. The fluxes are

$$J_{LCC} = \kappa\cdot\frac{S\cdot g_{Ca}m_\infty(V - V_{Ca})}{2F}, \tag{3.19}$$

$$J_{mleak} = \frac{c_0^{mn_{pump}}}{K_{mpump}^{mn_{pump}} + c_0^{mn_{pump}}}, \tag{3.20}$$

$$J_{mpump} = \frac{c^{mn_{pump}}}{K_{m_{pump}}^{mn_{pump}} + c^{mn_{pump}}}. \tag{3.21}$$

The complete updated model is then made up of equations (3.2)–(3.5), (3.7), and (3.9)–(3.21).

Since the updated model uses partial differential equations, we apply the finite element method (FEM) in order to solve over a specific time period. FEM is a method of approximation used to solve systems of partial differential or nonlinear equations over even geometrically complicated domains. While real cells have membrane invaginations as T-tubules penetrating the cell to interact with CRUs, we consider a regular 3-dimensional grid of point-source-like CRUs as shown in Figure 3.1. Using a computer-based model, we are able to compute a finite element matrix and vector, though our implementation is

Parameters	Definition	Values/Units	Source
s_0	initial SR calcium concentration	1,000-10,000 μM	[5], [26]
nss	number of SR Ca^{2+} buffer species	1	
b_j	SR buffer concentrations	6000 μM	[5]
D_s	SR calcium diffusion coefficient matrix	diag(0.78,0.78,0.78) μm^2/ms	This work
D_{b_j}	SR buffer diffusion coefficient matrix	diag(0.01,0.01,0.01) μm^2/ms	[5, 25]
γ	ratio of volume of cytosol to SR	14	[20]
K_{prob_s}	sensitivity of CRU to open due to SR calcium	200,550 μM	This work

Table 3.2: Parameter values added to the updated model for SR calcium.

matrix-free [12]. The mathematical model is coded in C, run using parallel computing (MPI) to efficiently generate simulations of the model, and post-processed in Matlab.

4 Results

In order to visualize the data sets produced by our model, we utilize Matlab code to make three different types of images: line-scans, SR plots, and voltage/flux plots. For the line-scan, cytosol Ca^{2+} concentration (μM) is tracked along the center of the cell in the longitudinal direction at each millisecond, and then space is graphed vertically and time horizontally. The final image is colored based off of Ca^{2+} concentration from 0 to 5μM; red indicates high concentration and blue indicates low concentration. SR plots track SR Ca^{2+} concentration (μM/ms), c, along three different lines, left, center, and right, within the SR. Voltage/flux plots show the voltage across the cell membrane (mV) and Ca^{2+}flux (μM/ms) through the LCC channels at each millisecond, and overlay their graphs.

Based on our various additions to the model and their numerical implementation, we were able to produce numerous results indicating various types of Ca^{2+} dynamics. These results were grouped into three major behaviors: localized sparks, waves, or blowups. And the parameters we have chosen to manipulate have some effect on shifting between these three comprehensive dynamics. Figures 4.1(a), 4.2(a), and 4.3(a) depict example line-scan images of each behavior type.

Note that in Figure 4.1(a) there is an almost periodic sideways "V" shape to the lighter blue shades where Ca^{2+} concentration in the cytosol is higher in the cell. The farthest left point of a V implies Ca^{2+} release from the initial CRU, here in the middle of the cell, triggering Ca^{2+} release at nearby CRUs which also trigger Ca^{2+} release at CRUs nearby to them. This CICR moves farther and farther towards the end of the cell in each direction, in effect creating a wave of Ca^{2+} release in a "V" shape. Two other waves have initiated near each end of the cell and propagate toward the center until they collide with the centrally initiated wave and stop propagating. This Ca^{2+} release is reflected in Figure 4.1(b), the corresponding graph of SR Ca^{2+} load over time. The downward spikes of the SR load correspond to the Ca^{2+} increase in the cytosol at the same time. Despite this decrease in SR load, however, the scale on the left, indicating SR load (μM) shows that the decreasing Ca^{2+} concentration stabilizes at about ~ 3000 μM.

Figure 4.2(a) shows small, spontaneous releases of Ca^{2+} over time. These are known as sparks because, although calcium was released, CICR-triggered wave propagation did not occur. In the corresponding SR plot, Figure 4.2(b), the downward spikes in SR again correspond to small increases in Ca^{2+} concentration in the cytosol. Take note, as well, that the scaling in Figure 4.2(a), the scale for concentration levels, has a smaller range than that in Figures 4.1(a) and 4.3(a), as the concentration increases during spark dynamics are much more minimal. This explains why no further sparks, and thus no CICR,

Parameters	Definition	Values/Units	Source
I_{app}	applied current	10 μA/cm^2	[18]
C	membrane capacitance	20 μF/cm^2	[18]
g_L	max./instantaneous conductance for leak	2 mmho/cm^2	[18]
g_{Ca}	max./instantaneous conductance for Ca^{2+}	4 mmho/cm^2	[18]
g_K	max./instantaneous conductance for K^+	8 mmho/cm^2	[18]
V_L	equilibrium potential for leak conductance	-50 mV	[18]
V_{Ca}	equilibrium potential for Ca^{2+} conductance	100 mV	[18]
V_K	equilibrium potential for K^+ conductance	-70 mV	[18]
λ_n	max. rate constant for K^+ channel opening	s^{-1}	[18]
S	surface area of the cell	3604.48 μm	[12]
mn_{pump}	membrane pump hill coefficient	2	assumed
K_{mpump}	membrane pump Ca^{2+} sensitivity parameter	0.18	estimated from SR pump
V_1	potential at which $M_\infty = 0.5$	-1 mV	[18]
V_2	reciprocal of slope of voltage dependence of M_∞	15 mV	[18]
V_3	potential at which $N_\infty = 0.5$	10 mV	[18]
V_4	reciprocal of slope of voltage dependence of N_∞	4.5 mV	[18]
τ	scaling factor of Morris-Lecar model to fit AP duration	0.1 μM μm^3/ms	This work
κ	scaling factor of J_{LCC}	0.01	This work

Table 3.3: Parameter values added to the updated model for Morris-Lecar voltage equations.

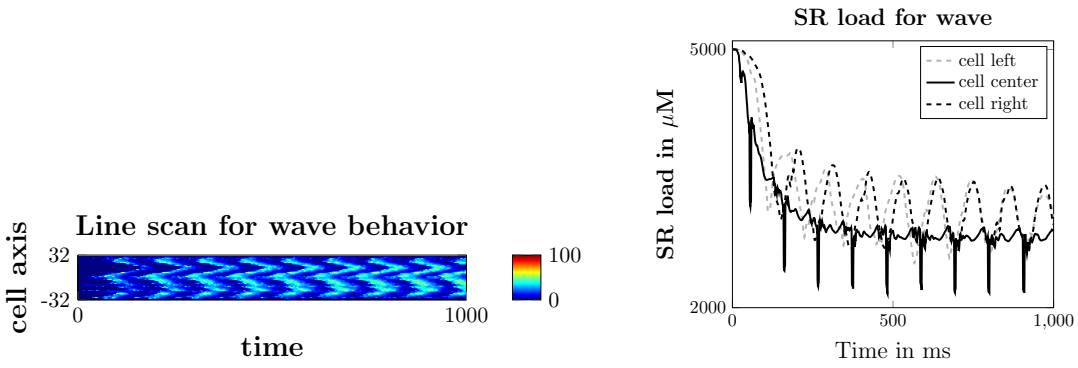

(a) (b)

Figure 4.1: Calcium Waves. (a) Integrated calcium concentration along the y-depth (line scan) at $x = 0$ μm shows initiation of waves at about 100 ms located at about -30, 0, 30 μm on the z-dimension. These propagate and collide after about 100 ms but reinitiate again and again. (b) Corresponding SR calcium levels at about -20 (left), 0 (center), and 20 (right) μm. After a transit equilibration SR load dips when calcium leaves the SR and increases when calcium is taken back up into the SR. Note: Periodicity induced by CRU recovery timescale. $\hat{\sigma} = 150$ μMμm^3/ms, $s_0 = 5000$ μM, $K_{prob_c} = 10$ μM.

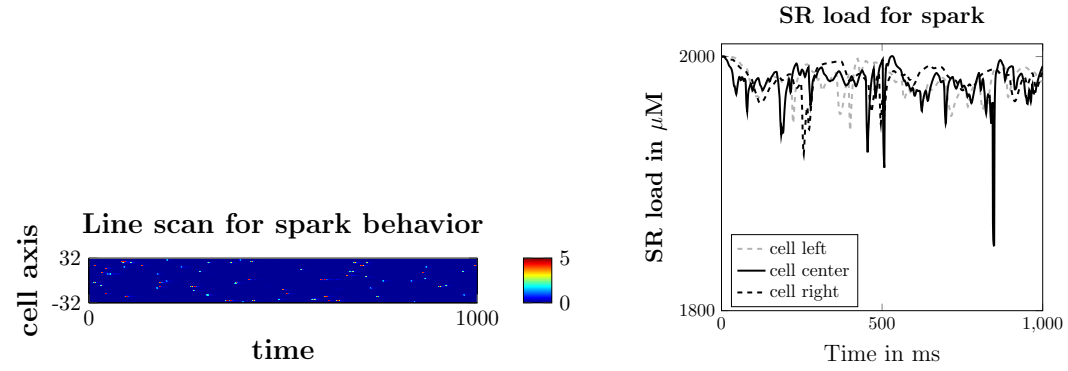

(a) (b)

Figure 4.2: Calcium Sparks. (a) Points of slightly elevated calcium released at CRUs but not propagating. (b) Corresponding SR dips during sparks. $\hat{\sigma} = 200$ μMμm^3/ms, $s_0 = 2000$ μM, $K_{prob_c} = 15$ μM.

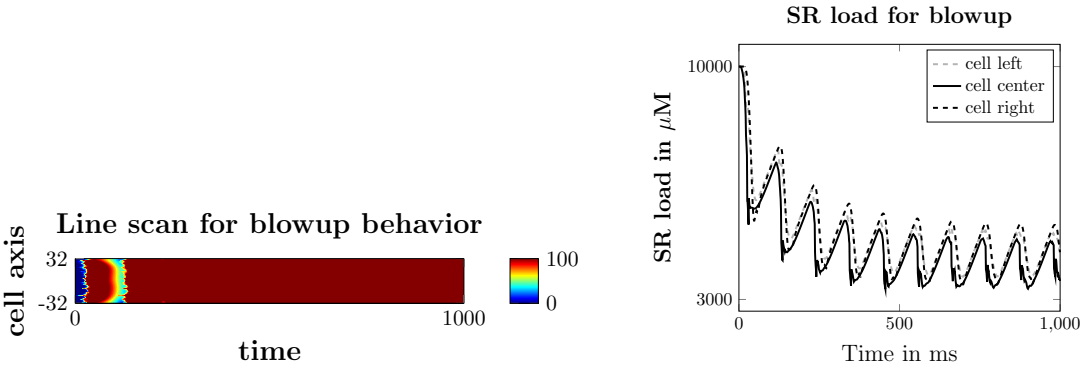

(a) (b)

Figure 4.3: Calcium Blow-up. (a) Calcium continues to rise without recovery due to high SR load. (b) Periodic SR release and uptake. Note: Periodicity due to CRU recovery timescale. $\hat{\sigma} = 200$ μMμm^3/ms, $s_0 = 10000$ μM, $K_{prob_c} = 5$ μM.

is triggered.

Figure 4.3(a) shows a quick, massive increase in Ca^{2+} in the cytosol that is never recovered back into the SR. This is what we call a blowup, because Ca^{2+} floods the cytosol and the pumps to the SR and extracellular space cannot act quickly enough in order to remove it. Figure 4.3(b) shows this failure to pump Ca^{2+} back into the SR with its dramatic decrease in SR Ca^{2+} load over time, as depicted on the left scale, with a decrease to about 30% of the starting concentration. While the level does equilibrate to a regular rhythm of release and uptake based on CRU recovery timescale, the cytosolic level is deemed too large for physiological function. This is in contrast to the result in [8] where with the static SR and without SR depletion cytosolic calcium rise will continue relating to a true "blow-up" state. This is one key result of this additional to the model.

Figure 4.4(a) shows how we use τ to make the oscillations of the voltage match the timing of the action potential and how we use κ to scale the flux appropriately. Figure 4.4(b) contrasts a line-scan from a run assuming that LCCs are everywhere in the cell membrane, to a line-scan from a run assuming that LCCs are found only near CRUs, Figure 4.4(c). The line scan images show that with the LCCs juxtaposed with the CRU rather than dispersed, the propagation is better organized showing a stronger "V" shape. In order to preserve the same overall calcium flux through the cell membrane for every simulation, flux through each LCC in the model assuming that LCCs are everywhere will be less than that of the LCCs in the CRU-limited model, as shown in Figure 4.4(a).

After we implemented the SR and its buffers into the model, we wanted to compare calcium dynamics with and without buffers in the SR as we changed certain parameters. The addition of buffers has the effect of shifting the quantitative thresholds of the transitions between calcium dynamics predictably [8], so we do not show those results. Figure 4.5 represents simulations under conditions with no buffers, with the different parameter sets we chose to fill in the values for K_{prob_c}, $\hat{\sigma}$, SR calcium load, s_0, diffusion coefficient, D_{SR}, and K_{prob_s}, each found from researching cardiac cells of different animals. These same parameters were used with simulations involving buffers. Every small colored square represents one simulation. Each parameter had multiple values, $K_{prob_c} \in \{5, 10, 15\}$ μM/ms, $\hat{\sigma} \in \{100, 150, 180, 200\}$ μMμm^3/ms, $s_0 \in \{1000, 2000, 5000, 10000\}$ μM, $D_{SR} \in \{0.08, 0.20, 0.78\}$ μm^2/ms, $V_{pump} \in \{2, 4, 6\}$ μM/ms, and $K_{prob_s} \in \{200, 550\}$ μM/ms.

In Figure 4.5 we found that V_{pump} has a significant effective on calcium dynamics where the lower level $V_{pump} = 2$ μM/ms allows for the full range of calcium dynamics. For this value of V_{pump} with large SR diffusion sparks, waves, and blow-up were found as SR load increases for the range of $\hat{\sigma}$ (Sigma in Figures 4.5 and 4.6) and K_{prob_c} and whether or not release was very sensitive to SR calcium (e.g., in Figure 4.6). These multiparameteric tables effectively act as multidimensional bifurcation diagrams allowing an efficient visual search through parameter space to find delineations of qualitatively different biophysical solutions. These extend similar images in [8], e.g., Figure 6 in that work.

5 Discussion

5.1 SR Calcium Load

We have taken a model by Izu et al. [13, 14] implemented by Gobbert [12] and extended by Coulibaly et al. [8] in equations (3.1)–(3.8), and extended it to include a dynamic calcium store in the SR and a basic electrical model that provides an influx of calcium with depolarization in the Morris-Lecar model [18] written in equations (3.13)–(3.21). After including the effects of a dynamic SR calcium concentration in the mathematical model and adapting the given equations (3.11) and (3.12), we observed the resulting Ca^{2+} dynamics, through line-scan images similar to those in Figures 4.1(a), 4.2(a), and 4.3(a). We found that we get similar calcium dynamics as without dynamic SR calcium but that with a dynamic SR even if calcium levels rise beyond physiological levels, as in blow-up, they must be capped.

With the calcium dynamic types given with $K_{prob_s} = 550$ in Figure 4.5 and $K_{prob_s} = 200$ in Figure 4.6, we were able to consider the effect of several parameters. When K_{prob_s} was decreased, the production of waves became more likely. This trend makes sense within the biological model, as K_{prob_s} signifies the CRU sensitivity to SR Ca^{2+} concentration, so a lower sensitivity value means that the CRU will be more likely to open and allow Ca^{2+} to enter into the cytosol, because it has a lower Ca^{2+} concentration at which it opens.

Similarly to the CRU sensitivity to SR Ca^{2+}, when K_{prob_c}, the CRU sensitivity to cytosolic Ca^{2+}, increases, waves occur less often. This also aligns with the biological model, as the CRUs are less likely to open until higher concentrations of cystolic Ca^{2+} are reached.

When V_{pump} is increased, waves occur less under conditions that are otherwise the same. This also aligns with the biological phenomena. Since V_{pump} is the strength of the pump that pulls Ca^{2+} back into the SR, a higher value will mean that the Ca^{2+} is taken back more quickly into the SR and then is not available to trigger other CRUs to spark.

Increasing D_s brought about waves more often. Though this seems strange since this diffusion is only of the Ca^{2+} within the SR, if Ca^{2+} moves about more easily within the SR then it may be more likely to reach the

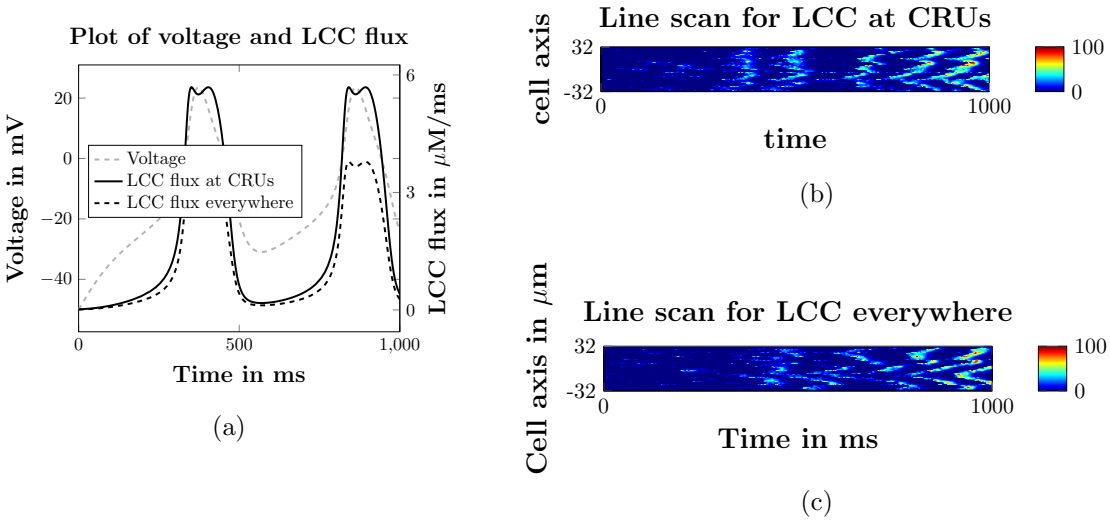

Figure 4.4: Cell Voltage and Calcium Influx Located at CRUs or Uniformly Distributed. (a) Voltage trace from the Morris-Lecar electrical model and the calcium influx from calcium channels either localized to the CRUs or distributed uniformly. (b) Line scan from Calcium channels localized to CRUs. (c) Line scan from calcium channels uniformly distributed. $\hat{\sigma} = 150$ μMμm^3/ms, $s_0 = 5000$ μM, $K_{prob_c} = 10$ μM, $D_{SR} = 0.78$ μm^2/ms, $V_{pump} = 4$ μM/ms.

CRU and travel through it into the cytosol, thus increasing the cytosolic Ca^{2+} concentration.

Increased s_0 also shows an increased occurrence of waves. This was also in alignment with the biological model, as an increased concentration of Ca^{2+} in the SR at the same K_{prob_s} would cause the CRUs to open and fire more often.

Waves also became more common as $\hat{\sigma}$ increased, aligning with intuition based upon the biological background. As the maximum release rate through the CRUs increased, then more Ca^{2+} would flow into the intracellular space per unit time.

When the SR was loaded with high Ca^{2+} concentration ($s_0 = 10000$ μM) and high SR diffusion coefficient ($D_s = 0.78$ μm^2/ms) at low strength of the SR pump ($V_{pump} = 2$ μM/ms), the cytosol floods with Ca^{2+} to the point where the pump, since it is so weak, is unable to respond by clearing cytosolic calcium. At these high concentrations, when $\hat{\sigma}$ was a higher value, since the rate by which Ca^{2+} left the SR and entered the intracellular space was higher, the simulated cell presented a similar inability to recover from these high concentrations of Ca^{2+}.

5.2 SR Buffers

Upon including a buffer species, particularly calsequestrin, in the SR, the simulation results resulted in less wave occurrences and less blow-outs under the conditions specified in Section 5.1, compared to those from simulations run before including an SR buffer (Figures 4.5 and 4.6).

Since SR buffers decrease the concentration of free SR calcium available to signal CRUs to open in equation (3.3), we expect the presence of wave dynamics to decrease dramatically. Keeping the parameters constant, most runs that produced waves without buffers showed a spark dynamic with buffers included, as predicted. However, likely due to the parameter discretization, we observed few waves with the buffered simulations, even those which exhibit a major blowup without buffers, as depicted in Figures 4.5 and 4.6.

5.3 Voltage: Morris-Lecar Model

After implementing the Morris-Lecar Model (Section 3.2.1) and looking over our previous simulations, we chose a set of calcium handling parameters to run that had only produced sparks previously. Since including voltage means that cytosol Ca^{2+} concentration would further increase, this intuitively meant we would be more likely to see waves on this set of parameters. Our first few runs produced voltage/flux plots like Figure 4.4, where τ successfully fit the voltage to the flux at LCCs. After these runs, however, we quickly realized that the calcium influx was unrealistically large resulting in a blow-up dynamic for most parameters.

To counter this unrealistic behavior, we implemented κ in equation (3.19) in order to counteract the overflow of extracellular calcium into the cell. With the inclusion of this parameter, and with increased J_{mpump}, we were able to manipulate the simulation to produce some wave-like behavior as shown in Figure 4.4. Note that, in these im-

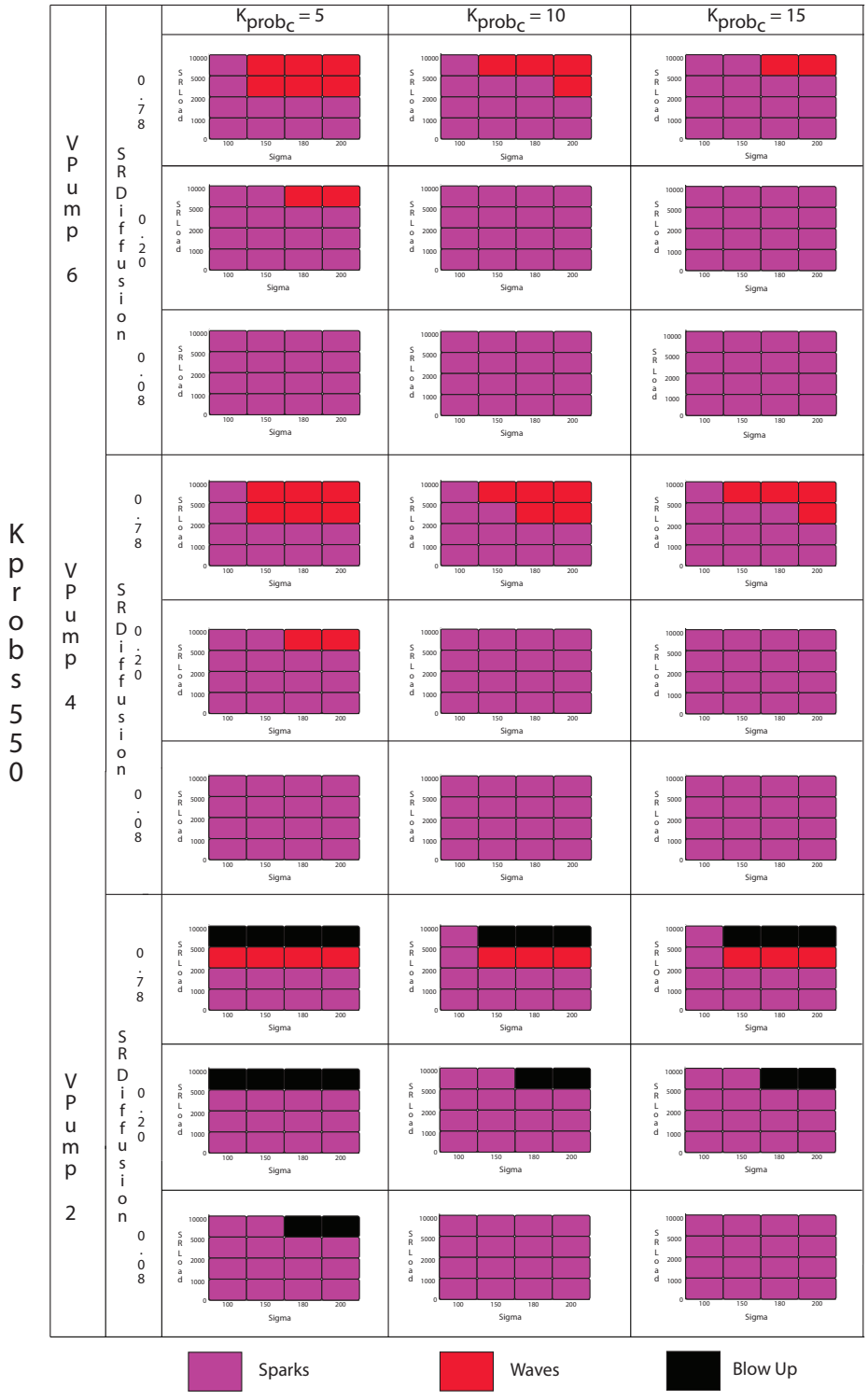

Figure 4.5: Sparks, Waves, or Blow-up Low SR release sensitivity. For several sets of parameters either sparks, propagated waves, or calcium blow was recorded. SR without buffers and $K_{prob_s} = 550$.

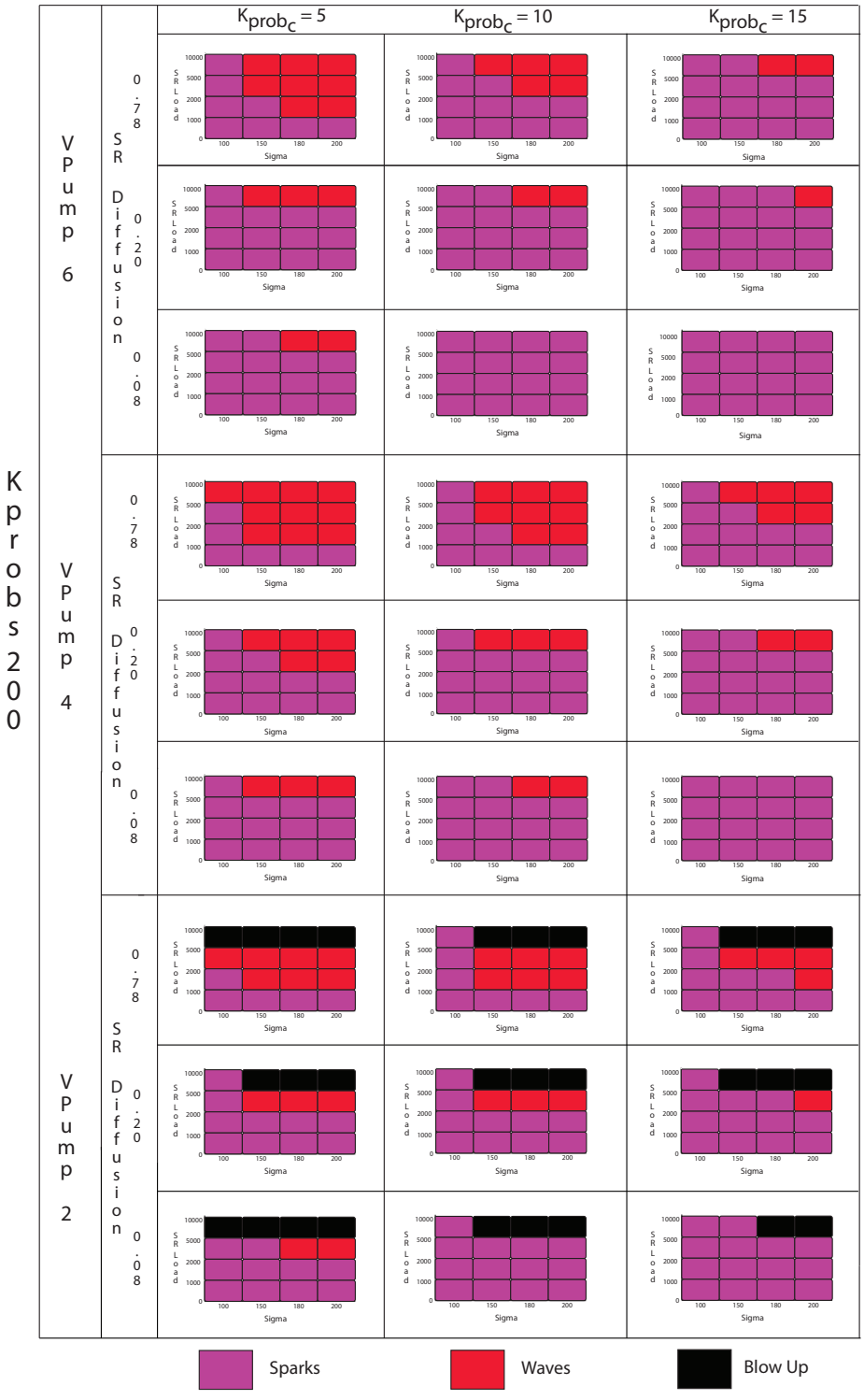

Figure 4.6: Sparks, Waves, or Blow-up High SR release sensitivity. For several sets of parameters either sparks, propagated waves, or calcium blow was recorded. SR without buffers and $K_{prob_s} = 200$.

ages, we again see cytosol Ca^{2+} concentration increasing at the same time as a voltage spike.

For the flux plots in Figure 4.4, the later appearance of waves in 4.4(b) as compared with that 4.4(c) corresponds to the diffusion of Ca^{2+} entering the cell through the individual LCCs to reach the CRUs elsewhere thus beginning the process of CICR, since the LCCs are everywhere in the cell as opposed to directly across from the CRUs. In the case of 4.4(b), since the LCCs are directly across from the CRUs with greater flux entering the cell from the extracellular space, then CICR is more easily triggered with the same pump sensitivity.

6 Conclusions

Based on our simulation observations, we have been able to make various conclusions regarding the influence of the extensions we implemented in the original mathematical model [14]. Increasing initial SR Ca^{2+} concentration increases probability of calcium waves, though flooding of the cell can occur with a higher SR Ca^{2+} diffusion coefficient and low strength of the SR pump that pulls Ca^{2+} back into the cell. The addition of a buffer into the SR behaved as expected, decreasing the likelihood of wave propagation. Also as expected, we saw an increased probability of wave dynamics and, even more likely, calcium flooding in the cell when the voltage difference across the plasma membrane was included in the model. Overall, our findings aligned with known biological models and principles, giving us a thorough understanding of several factors that influence Ca^{2+} dynamics in cardiac myocytes.

Acknowledgments

These results were obtained as part of the REU Site: Interdisciplinary Program in High Performance Computing (`hpcreu.umbc.edu`) in the Department of Mathematics and Statistics at the University of Maryland, Baltimore County (UMBC) in Summer 2015. This program is funded by the National Science Foundation (NSF), the National Security Agency (NSA), and the Department of Defense (DOD), with additional support from UMBC, the Department of Mathematics and Statistics, the Center for Interdisciplinary Research and Consulting (CIRC), and the UMBC High Performance Computing Facility (HPCF). HPCF is supported by the U.S. National Science Foundation through the MRI program (grant nos. CNS–0821258 and CNS–1228778) and the SCREMS program (grant no. DMS–0821311), with additional substantial support from UMBC. Co-author Michael McCauley was supported, in part, by the UMBC National Security Agency (NSA) Scholars Program through a contract with the NSA. Graduate assistant Zana Coulibaly was supported during Summer 2015 by UMBC.

References

[1] C. Antzelevitch and S. Sicouri. (1994). Clinical relevance of cardiac arrhythmias generated by afterdepolarizations, *Journal of the American College of Cardiology*, **23**, 259–77.

[2] C. W. Balke and L. Goldman. (2003). Excitation contraction coupling in cardiac muscle, *Journal of General Physiology*, **121**, 349–52.

[3] D. M. Bers (2001). Excitation-Contraction Coupling and Cardiac Contractile Force. 2nd ed. *Dordrecht, The Netherlands: Kluwer Academic Publishers.*

[4] P. A. Boyden and H. E. ter Keurs. (2001). Reverse excitation-contraction coupling: Ca2+ ions as initiators of arrhythmias, *Journal of Cardiovascular Electrophysiology* **12**, 382–5.

[5] M. B. Cannell, C. H. T. Kong, M. S. Imtiaz, and D. R. Laver. (2013). Control of sarcoplasmic reticulum Ca^{2+} release by stochastic RyR gating within a 3D model of the cardiac dyad and importance of induction decay for CICR termination, *Biophysical Journal*, **104**, 2149–59.

[6] W. A. Catterall. (2011). Voltage-gated calcium channels, *Cold Spring Harbors Perspectives in Biology*, **3**, 1–23.

[7] H. Cheng, W. J. Lederer, and M. B. Cannell. (1993). Calcium sparks: elementary events underlying excitation-contraction coupling in heart muscle, *Science*, **262**, 740–4.

[8] Z. Coulibaly, M. K. Gobbert, and B. E. Peercy. (2014). Insight into spontaneous recurrent calcium waves in a 3-D cardiac cell based on analysis of a 1-D deterministic model, *International Journal of Computer Mathematics*, **92**, 591–607.

[9] M. E. Diaz, A. W. Trafford, S. C. O'Neill, and D. A. Eisner. (1997). Measurement of sarcoplasmic reticulum Ca2+ content and sarcolemmal Ca2+ fluxes in isolated rat ventricular myocytes during spontaneous Ca2+ release, *Journal of Physiology*, **501**, 3–16.

[10] L. E. Ford and R. J. Podolsky. (1970). Regenerative calcium release within muscle cells, *Science*, **167**, 58–9.

[11] J. A. Gilabert. (2012). Calcium signaling, *Advances in Experimental Medicine and Biology*, **740**, 483–98.

[12] M. K. Gobbert. (2008). Long-time simulations on high resolution meshes to model calcium waves in a heart cell, *SIAM Journal of Scientific Computing*, **30**, 2922–47.

[13] L. T. Izu, S. Means, J. Shadid, Y. Chen-Izu, and C. W. Balke. Interplay of ryanodine receptor distribution and calcium dynamics, *Biophysical Journal*, **91**, 95–112.

[14] L. T. Izu, W. G. Wier, and C. W. Balke. (2001). Evolution of cardiac calcium waves from stochastic calcium sparks, *Biophysical Journal*, **80**, 103–20.

[15] R. P. Katra and K. R. Laurita. (2005). Cellular mechanism of calcium-mediated triggered activity in the heart, *Circulation Research*, **96**, 535–42.

[16] Y. S. Lee and J. P. Keener. (2008). A calcium-induced calcium release mechanism mediated by calsequestrin, *Journal of Theoretical Biology*, **253**, 668–79.

[17] A. R. Marks. (2003). Calcium and the heart: a question of life and death, *Journal of Clinical Investigation*, **111**, 597–9.

[18] C. Morris and H. Lecar. (1981). Voltage oscillations in the barnacle giant muscle fiber, *Biophysical Journal*, **35**, 193–213.

[19] E. Picht, A. V. Zima, T. R. Shannon, A. M. Duncan, L. A. Blatter, and D. M. Bers. (2011). Dynamic calcium movement inside cardiac sarcoplasmic reticulum during release, *Circulation Research*, **108**, 846–56.

[20] H. R. Ramay, M. S. Jafri, W. J. Lederer, and E. A. Sobie. (2010). Predicting local SR Ca2+ dynamics during Ca2+ wave propagation in ventricular myocytes, *Biophysical Journal*, **98**, 2515–23.

[21] S. Ringer. (1883). A further contribution regarding the influence of the different constituents of the blood on the contraction of the heart, *Journal of Physiology*, **4**, 29–42.

[22] J. Sanderson. (1996). The SWORD of Damocles, *The Lancet* **348**, 2–3.

[23] Shannon T.R., K.S. Ginsburg, D.M. Bers. (2002). Quantitative assessment of the SR Ca2+ leak-load relationship, *Circ Res*, **91**, 594–600.

[24] Y. Shiferaw, G. L Aistrup, and J. A. Wasserstrom. (2012). Intracellular Ca^{2+} waves, afterdepolarizations, and triggered arrhythmias, *Cardiovascular Research*, **95**, 265–8.

[25] G. Smith and N. MacQuaide. (2008). Cytoplasmic versus intra-SR: the battle of the Ca2+ diffusion coefficients in cardiac muscle, *Biophysical Journal*, **95**, 1005–6.

[26] P. Swietach, K. W. Spitzer, and R. D. Vaughan-Jones. (2008). Ca2+-mobility in the sarcoplasmic reticulum of ventricular myocytes is low, *Biophysical Journal*, **95**, 1412–27.

[27] P. Swietach, K. W. Spitzer, and R. D. Vaughan-Jones. (2010). Modeling calcium waves in cardiac myocytes: importance of calcium diffusion, *Front Biosci (Landmark Ed)*, **15**, 661–80.

[28] J, N. Weiss, A. Garfinkel, H. S. Karagueuzian, P. Chen, and Q. Zhilin. (2010). Early afterdepolarizations and cardiac arrhythmias, *Heart Rhythm Society*, **7**, 1891–9.